ELSEVIER

Journal of Nuclear Materials 280 (2000) 206–215

journal of nuclear materials

www.elsevier.nl/locate/jnucmat

Single-pass flow-through experiments on a simulated waste glass in alkaline media at 40°C. II. Experiments conducted with buffer solutions containing controlled quantities of Si and Al

Paul K. Abraitis [a,*], B.P. McGrail [b], D.P. Trivedi [c], F.R. Livens [d], D.J. Vaughan [a]

[a] *Department of Earth Sciences, The University of Manchester, The Williamson Building, Oxford Road, Manchester M13 9PL, UK*
[b] *Department of Applied Geology and Geochemistry, Pacific Northwest National Laboratory, Richland, WA 99352, USA*
[c] *British Nuclear Fuels plc, Environmental Assessments, Risley, Warrington, Cheshire WA3 6AS, UK*
[d] *Department of Chemistry, The University of Manchester, Oxford Road, Manchester M13 9PL, UK*

Received 11 November 1999; accepted 6 March 2000

Abstract

Additional single-pass flow-through (SPFT) experiments have been conducted with a complex, simulated waste glass at 40°C in moderately alkaline media. Results are compared to those obtained in the experiments described in Part I, and with published data obtained in long-term, static, batch dissolution experiments with this glass formulation. Dissolution rate laws for the glass must account for the rate influencing effects of both dissolved Si and Al species. These experiments have shown that on a mole per mole basis, dissolved Al has a more significant influence on the glass dissolution rate than dissolved Si under these experimental conditions. The very low 'long-term' dissolution rates reported in static batch dissolution experiments reflect near saturation conditions that are not attained in SPFT tests as a result of solution flow-through.

PACS: 21.41.Kw; 82.55.+e; 82.20.wt; 82.70.Gg

1. Introduction

This work describes the results of a series of systematic experiments to objectively evaluate the controls on the dissolution rate of a simulated waste glass in moderately alkaline media at 40°C. This non-radioactive borosilicate contains a complex mixture of simulated fission product oxides with a composition similar to that generated during Magnox fuel reprocessing. Experiments have utilised a single-pass flow-through (SPFT) apparatus [1].

In Part I [2], the results of SPFT experiments were presented in which the solution flow rate and glass surface area were systematically varied across the experimental matrix using the same input buffer solution in each test. The solution composition within the reaction cells was influenced only by glass-solution reactions and secondary processes (including the development of secondary reaction products). The results indicate that surface reaction-controlled dissolution of this complex glass is congruent under these experimental conditions. Dissolution is accompanied by the formation of secondary Al–K–Fe–Mg–Si-bearing gels under test conditions where higher concentrations of glass derived solutes accumulate in solution.

The findings described in Part I also indicate that the rate of dissolution is influenced by dissolved Al and Si species. The experimental dissolution rates are consistent with a rate law containing an activity product term including both Al and Si species ($a^{0.06}_{Al(OH)^-_4(aq)} \cdot a^{0.51}_{H_4SiO_4}$).

* Corresponding author. Tel.: +44-161 275 7489; fax: +44-161 275 3947.
E-mail address: pabraitis@fs1.ge.man.ac.uk (P.K. Abraitis).

0022-3115/00/$ - see front matter
PII: S0022-3115(00)00040-4

The additional experiments described in this paper were designed to systematically evaluate the effects of dissolved Si and Al on the glass dissolution rate at constant flow rate (q, $m^3\ s^{-1}$) to glass surface area (s, m^2) ratio. Input buffer solutions differed in each case such that the dissolved Al and Si concentrations varied significantly across the experimental test matrix. The experiments were designed to isolate the dissolution rate influencing effects of dissolved Al and Si at constant pH and temperature. An additional series of experiments were conducted in which ethylenediamine tetra-acetic acid (EDTA) was present in the buffers to complex dissolved Al.

The experimental data and model predictions are compared with those described in Part I, and with published data obtained in long-term, static, batch dissolution experiments with this glass [3–5].

2. Experimental methodology

2.1. Single-pass flow-through experiments

The nature of the glass and the design of the experimental apparatus used in this study were described in Part I [2].

Three sets of 16 experiments were performed for periods of between 12 and 15 days. Experimental details are summarised in Table 1. The solution flow rate and the mass of glass in the reaction cell were effectively equal in each experiment within a given set. Thus each experiment within a given set was conducted at the same nominal q/s ($m\ s^{-1}$) ratio, whilst the input solution concentrations of Si and Al were varied independently across the experimental matrix.

Buffer solutions were prepared using a base buffer comprising a solution of 0.00018 M KOH (Apache Chemicals) + 0.005 M KCl (Baker). Additional ingredients were added to this base buffer mixture to generate solutions with the required chemistry. Concentrated 'stock' Si and Al solutions were prepared from analytical grade $Na_2SiO_3 \cdot 5H_2O$ (Sigma) and $Al(NO_3) \cdot 5H_2O$ (Baker) reagents, respectively. The pH of each of these solutions was adjusted to the base buffer pH (10.25) via addition of NaOH and HNO_3. For the MW-EDTA experiments a pH-adjusted EDTA solution was prepared from analytical grade Na_2EDTA (Fischer Scientific).

In the MW-Si experiments the input Si concentrations ranged from 0 to 55 mg l^{-1} Si. In the MW-Al experiments the input Al concentrations ranged from 0 to 0.9 mg l^{-1}. In the MW-EDTA experiments input Si concentrations ranged from 0 to 59 mg l^{-1} Si and Na_2EDTA was added to the KOH/KCl buffer mixture resulting in an EDTA concentration of 0.005 M.

The MW-Si and MW-EDTA experiments were conducted at a nominal q/s ratio of 8×10^{-8} m s^{-1}. The MW-Al experiments were conducted at a higher nominal q/s ratio of 2×10^{-7} m s^{-1}. The higher q/s ratio was used in the MW-Al experiments to ensure that Si concentrations in the reaction cells remained low.

Following collection, all solution samples were acidified to 1% nitric acid (Fisher Ultrex grade) and subsequently analysed by ICP-AES. Aluminium was below practical detection limits (20 μg l^{-1}) in many of the MW-Si experiments.

2.2. Rate determination

The pH-corrected normalised dissolution rates (g m^{-2} d^{-1}) reported in this study have been calculated using the expressions given in Part I (Section 2.4). All rate measurements are based on 'steady-state' boron concentrations in the reaction cell output solutions.

Table 1
Solution compositions in the MW-Si, MW-Al and MW-EDTA SPFT experiments

Experiment ID	Buffer composition	pH range[a]	[Si] range (mg l^{-1})[b]	[Al] range (μg l^{-1})[b]
MW-Si	1.8×10^{-4} M KOH 5.0×10^{-3} M KCl + $Na_2SiO_3 \cdot 5H_2O$	9.83–9.50	2–55	<DL–132[c]
MW-Al	1.8×10^{-4} M KOH 5.0×10^{-3} M KCl + $Al(NO_3)_3 \cdot 5H_2O$	10.23–9.97	0.8–1.21	169–429
MW-EDTA	1.8×10^{-4} M KOH 5.0×10^{-3} M KCl 5.0×10^{-3} Na_2EDTA + $Na_2SiO_3 \cdot 5H_2O$	10.50–10.23	9–66	46–338

[a] pH measured at room temperature (modelled pH values at 40°C are 0.46 pH units lower [2]).
[b] Concentration in the output solution determined by ICP-AES.
[c] Concentration less than the detection limit (20 μg l^{-1}, Pool [17]).

3. Results and discussion

3.1. Solution compositions and modelling

The chemistry of the solutions used in these experiments is summarised in Table 1. Dissolution rates, solution pH values and modelled activities of H_4SiO_4 and $Al(OH)_4^-(aq)$ in each experiment are shown in Tables 2–4. The rate and solution activity values shown in these tables are based on analyses of the final three solution samples collected from each reaction cell.

Because of the differing chemistries of the buffer solutions used in these experiments, it was not possible to exactly match solution pH values between the different sets of experiments. However, pH variations were generally small within a given set of the experiments (maximum pH variation being observed in the MW-Si experiments with a range of 0.33 pH units). As shown in Table 1, pH values ranged between 9.04 and 9.37 in the MW-Si experiments, 9.51–9.71 in the MW-Al experiments and 9.97–10.04 in the MW-EDTA experiments.

Given these differences in pH and buffer solution composition, it is important to assess the speciation of Si and Al in each set of experiments. Fig. 1 shows the modelled distribution of the major Si and Al species in the buffer solutions used in this study. Geochemical modelling calculations using PHREEQC [6] suggest that the dominant Si species in each experiment are the undissociated silicic acid molecule (H_4SiO_4) and the conjugate base ($H_3SiO_4^-(aq)$), the latter dominating in the

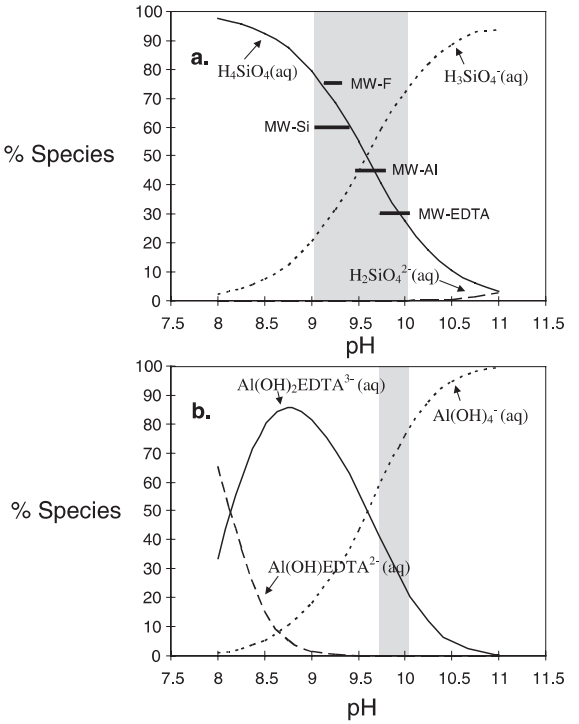

Fig. 1. Speciation of Si and Al in the buffer solutions: (a) mol% of major aqueous Si species in a KOH/KCl buffer solution containing 5 mg l^{-1} Si in the pH range 8–11 at 40°C (bars denote the pH range in each set of experiments) and (b) mol% of the major aqueous Al species in a KOH/KCl buffer solution containing 0.005 M Na_2EDTA + 0.5 mg l^{-1} Al in the pH range 8–11 at 40°C (the shaded region shows the pH range in the MW-EDTA experiments).

Table 2
Data from the MW-Si experiments

Test ID	$\log_{10} q/s$ (m s^{-1})	pH[a]	Rf[b]	Rate (g m^{-2} d^{-1})[c]	$Al(OH)_4^-$[d]	H_4SiO_4[d]
MW-Si_1	−7.11	9.33	1.056	0.084 ± 0.009	4.52×10^6	4.56×10^5
MW-Si_2	−7.11	9.37	1.015	0.082 ± 0.011	4.52×10^6	6.20×10^5
MW-Si_3	−7.12	9.21	1.176	0.078 ± 0.107	3.77×10^6	8.55×10^5
MW-Si_4	−7.12	9.37	1.015	0.088 ± 0.009	5.26×10^6	8.37×10^5
MW-Si_5	−7.12	9.35	1.034	0.088 ± 0.008	3.26×10^6	9.98×10^5
MW-Si_6	−7.13	9.12	1.280	0.131 ± 0.008	1.88×10^6	1.50×10^4
MW-Si_7	−7.12	9.04	1.383	0.131 ± 0.002	1.88×10^6	1.70×10^4
MW-Si_8	−7.16	9.23	1.162	0.124 ± 0.009	1.38×10^6	2.57×10^4
MW-Si_9	−7.12	9.12	1.281	0.166 ± 0.043	–	3.96×10^4
MW-Si_10	−7.13	9.04	1.387	0.192 ± 0.051	–	5.43×10^4
MW-Si_11	−7.13	9.06	1.357	0.223 ± 0.398	–	6.23×10^4
MW-Si_12	−7.11	9.06	1.362	0.163 ± 0.012	–	7.88×10^4
MW-Si_13	−7.13	9.04	1.389	0.144 ± 0.041	–	8.75×10^4
MW-Si_14	−7.14	9.08	1.339	0.153 ± 0.016	–	1.01×10^3
MW-Si_15	−7.12	9.07	1.348	0.138 ± 0.023	–	1.31×10^3
MW-Si_16	−7.14	9.06	1.381	0.129 ± 0.020	–	1.50×10^3

[a] Estimated pH at 40°C, given by the measured pH (at room temperature) minus 0.46 pH units.
[b] Rate correction factor [2].
[c] Mean pH corrected rate of glass dissolution based on steady-state B output concentrations, uncertainties are 95% confidence limits ($n = 3$).
[d] Activities modelled using PHREEQC [6].

Table 3
Data from the MW-Al experiments

Test ID	$\log_{10} q/s$ (m s^{-1})	pH[a]	Rf[b]	Rate (g m^{-2} d^{-1})[c]	$a_{(Al(OH)_4^-}$[d]	$a_{H_4SiO_4}$[d]
MW-Al_1	−6.63	9.51	0.891	0.104 ± 0.001	5.77×106	3.66×10^5
MW-Al_2	−6.65	9.72	0.730	0.069 ± 0.003	5.58×10^6	1.61×10^5
MW-Al_3	−6.67	9.66	0.769	0.074 ± 0.003	6.52×10^6	1.84×10^5
MW-Al_4	−6.67	9.71	0.733	0.076 ± 0.003	7.70×10^6	1.92×10^5
MW-Al_5	−6.66	9.77	0.697	0.076 ± 0.001	8.49×10^6	1.77×10^5
MW-Al_6	−6.66	9.60	0.816	0.082 ± 0.001	8.56×10^6	1.18×10^5
MW-Al_7	−6.67	9.73	0.719	0.067 ± 0.003	9.02×10^6	1.68×10^5
MW-Al_8	−6.70	9.52	0.881	0.087 ± 0.001	9.46×10^6	2.39×10^5
MW-Al_9	−6.65	9.73	0.724	0.065 ± 0.008	9.32×10^6	1.99×10^5
MW-Al_10	−6.68	9.76	0.701	0.066 ± 0.003	9.75×10^6	1.61×10^5
MW-Al_11	−6.70	9.69	0.746	0.070 ± 0.003	1.08×10^{-5}	2.71×10^5
MW-Al_12	−6.68	9.55	0.856	0.080 ± 0.007	1.16×10^{-5}	1.95×10^5
MW-Al_13	−6.66	9.59	0.825	0.070 ± 0.002	9.58×10^6	1.62×10^5
MW-Al_14	−6.66	9.53	0.874	0.076 ± 0.002	1.27×10^5	1.75×10^5
MW-Al_15	−6.65	9.63	0.796	0.071 ± 0.002	1.42×10^5	1.45×10^5
MW-Al_16	−6.68	9.56	0.850	0.078 ± 0.011	1.55×10^5	1.44×10^5

[a] Estimated pH at 40°C, given by the measured pH (at room temperature) minus 0.46 pH units.
[b] Rate correction factor [2].
[c] Mean pH corrected rate of glass dissolution based on steady-state B output concentrations, uncertainties are 95% confidence limits ($n = 3$).
[d] Activities modelled using PHREEQC [6].

Table 4
Data from the MW-EDTA experiments

Test ID	$\log_{10} q/s$ (m s^{-1})	pH[a]	Rf[b]	Rate (g m^{-2} d^{-1})[c]	$a_{Al(OH)_4^-}$[d]	$a_{H_4SiO_4}$[d]
MW-EDTA_1	−7.11	10.04	0.537	0.198 ± 0.048	3.02×10^{-6}	4.02×10^{-6}
MW-EDTA_2	−7.12	10.02	0.547	0.200 ± 0.050	2.65×10^{-6}	7.62×10^5
MW-EDTA_3	−7.13	10.02	0.547	0.195 ± 0.048	5.95×10^{-6}	9.32×10^5
MW-EDTA_4	−7.13	10.03	0.543	0.177 ± 0.015	5.72×10^{-6}	9.45×10^5
MW-EDTA_5	−7.13	10.02	0.549	0.208 ± 0.040	4.86×10^{-6}	1.11×10^{-4}
MW-EDTA_6	−7.14	10.00	0.561	0.198 ± 0.023	1.16×10^{-6}	1.12×10^{-4}
MW-EDTA_7	−7.14	10.01	0.554	0.201 ± 0.052	4.95×10^{-6}	1.30×10^{-4}
MW-EDTA_8	−7.14	9.98	0.570	0.197 ± 0.026	2.97×10^{-6}	1.75×10^{-4}
MW-EDTA_9	−7.13	9.95	0.584	0.235 ± 0.046	4.02×10^{-6}	2.54×10^{-4}
MW-EDTA_10	−7.13	9.92	0.605	0.214 ± 0.036	1.72×10^{-6}	3.14×10^{-4}
MW-EDTA_11	−7.13	9.92	0.604	0.232 ± 0.049	2.34×10^{-6}	3.44×10^{-4}
MW-EDTA_12	−7.12	9.93	0.600	0.194 ± 0.048	1.30×10^{-6}	4.02×10^{-4}
MW-EDTA_13	−7.13	9.87	0.633	0.156 ± 0.085	1.16×10^{-6}	4.40×10^{-4}
MW-EDTA_14	−7.13	9.84	0.651	0.176 ± 0.024	7.67×10^{-7}	5.45×10^{-4}
MW-EDTA_15	−7.13	9.77	0.697	0.163 ± 0.030	4.31×10^{-7}	8.34×10^{-4}
MW-EDTA_16	−7.13	9.78	0.690	0.174 ± 0.056	7.74×10^{-7}	8.62×10^{-4}

[a] Estimated pH at 40°C, given by the measured pH (at room temperature) minus 0.46 pH units.
[b] Rate correction factor [2].
[c] Mean pH corrected rate of glass dissolution based on steady-state B output concentrations, uncertainties are 95% confidence limits ($n = 3$).
[d] Activities modelled using PHREEQC [6].

higher pH experiments. In the MW-Si experiments, the H_4SiO_4 species is predicted to dominate, comprising between approximately 60% and 80% of the total dissolved Si. In the MW-Al and MW-EDTA experiments, the anionic $H_3SiO_4^-(aq)$ species is important, comprising between approximately 30% and 40% and between 60% and 80% of the total Si, respectively.

In the MW-Si and MW-Al solutions, the major Al species is the tetrahydroxoaluminate anion ($Al(OH)_4^-(aq)$) and over 99% of the Al atoms in the

solution are predicted to be present in this form. Minor Al species include the neutral $Al(OH)_3^0(aq)$ species and the $Al(OH)_2^+(aq)$ cation. In the MW-EDTA solutions, additional Al-EDTA complexes are present. The predominant Al species in these solutions are $Al(OH)_4^-(aq)$ and $Al(OH)_2EDTA^{3-}(aq)$ anions. Geochemical modelling suggests that the $Al(OH)_4^-(aq)$ anion becomes increasingly important as the solution pH increases.

3.2. Results of the MW-Si experiments

Data from the MW-Si experiments are summarised in Table 2. The MW-Si experiments were conducted with a mean q/s ratio of 7.63×10^{-8} m s^{-1}. Variations in the solution flow rate over the duration of the experiments were minimal (RSD < 5%). Input solution pH values ranged from 9.04 to 9.37 (a spread of 0.33 pH units). As shown in Table 2, $\log_{10} q/s$ values in the MW-Si experiments ranged from −7.11 to −7.16. Output Si concentrations ranged from 2 to 55 mg l^{-1}. Al concentrations ranged from 40 to 132 μg l^{-1}, but in many cases the concentration of this element was below the ICP-AES detection limit.

Dissolved Al concentrations in the reaction cell output solutions generally decreased with increasing dissolved silica concentration. This suggests that Al concentrations were controlled by the development of a secondary, aluminosilicate phase (possibly a hydrosilicate gel), as identified in Part I. In the most Si-rich solutions precipitation of this phase within the cells resulted in output Al concentrations below ICP-AES detection limits.

3.3. Results of the MW-Al experiments

Data from the MW-Al experiments are summarised in Table 3. The mean q/s ratio in the MW-Al experiments was 2.19×10^{7} m s^{-1}. Input solution pH values ranged from 9.51 to 9.77 (a spread of 0.26 pH units). Output Al concentrations ranged from 169 to 429 μg l^{-1}. Steady-state Al concentrations were up to ten times higher than those in the MW-Si experiments, whilst the Si concentrations were in the range of 0.76–1.21 mg l^{-1}.

3.4. Results of the MW-EDTA experiments

Data from the MW-EDTA experiments are summarised in Table 4. The MW-EDTA experiments were conducted with a mean q/s ratio of 7.53×10^{8} m s^{-1}. Solution pH values ranged from 9.77 to 10.04 (with a spread of 0.27 pH units across the matrix). Output Si concentrations ranged from 9 to 66 mg l^{-1}. The output Al concentrations ranged from 46 to 338 μg l^{-1}.

As in the MW-Si experiments, there was a general negative correlation between the output Si and Al concentrations. However, in contrast with the MW-Si experiments, Al concentrations were above the ICP-AES detection limit in each MW-EDTA experiment. The enhanced solubility of Al in this solution matrix is consistent with the slightly higher solution pH and the formation of Al-EDTA complexes, as discussed in Section 3.1.

3.5. Rates of dissolution vs the activity of orthosilicic acid

In Fig. 2, rates of glass dissolution in the MW-Si experiments are plotted vs the activity of silicic acid. Dissolution rates generally decrease as the activity of orthosilicic acid increases in the MW-Si experiments where Al concentrations were below ICP-AES detection limits. However, in experiments where dissolved Al was present at quantifiable levels, the dissolution rates deviate significantly from this trend. It is clear from this plot that the dissolution rate does not show a simple linear dependence on silicic acid activity, as predicted by the model of Grambow [7], and this further confirms the findings of the MW-F experiments reported in Part I.

Fig. 3 shows a plot of the dissolution rates in the MW-Si and MW-EDTA experiments vs the activity of orthosilicic acid (data from the MW-Si_1 to MW-Si_8 experiments are not shown). The trendline in Fig. 3 is a line of best fit defined by linear regression of these data. This represents a fit to a Grambow style rate law [7] of the type

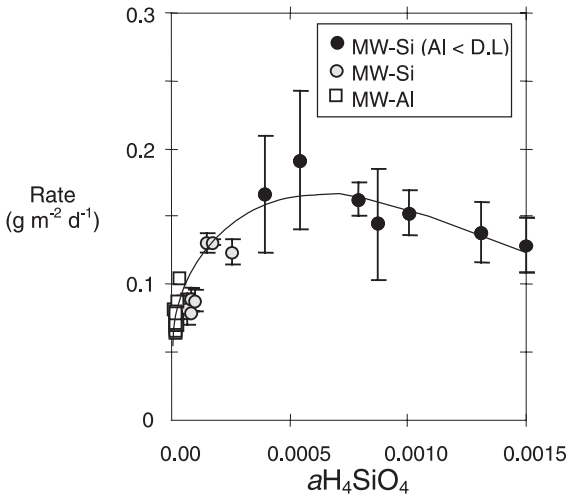

Fig. 2. Rates of glass dissolution (based on steady-state B concentrations) in the MW-Si and MW-Al experiments vs the activity of orthosilicic acid. Solid circles indicate dissolution rate data in the MW-Si experiments in which Al was below the ICP-AES detection limits (Al < DL). The trendline is shown as a guide for the eye, see text.

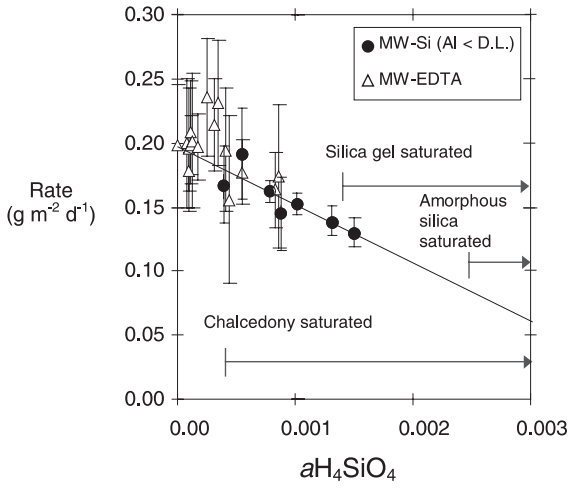

Fig. 3. Rates of glass dissolution (based on steady-state B concentrations) in the MW-Si and MW-EDTA experiments vs the activity of orthosilicic acid. The line shows a linear regression through the MW-Si data for tests in which Al was below the ICP-AES detection limits (Al < DL). Values of R_0 and aH_4SiO_{4Sat} are extrapolated by linear regression analysis (see text). Saturation with respect to chalcedony, silica gel and amorphous silica are shown.

$$r = k_+\left(1 - \frac{Q}{K}\right), \tag{1}$$

where r is the normalised dissolution rate (g m^{-2} d^{-1}), k_+ the dissolution rate constant at pH 9.38 and 40°C, Q the activity of silicic acid in solution ($a_{H_4SiO_4(aq)}$) and K is the activity of silicic acid at 'saturation'. Values of k_+ and K are estimated by linear regression at 0.196 ± 0.012 (g m^{-2} d^{-1}) and $4.35 \times 10^{-3} \pm 6.88 \times 10^{-4}$, respectively.

Saturation with respect to three potential secondary silica phases is also shown in Fig. 3. Thermodynamic modelling suggests that a number of the experimental systems are supersaturated with respect to chalcedony and near saturation with respect to silica gel. All systems are undersaturated with respect to amorphous silica (the most soluble silica phase in the data compilation of Nordstrom et al. [8]). Note that the extrapolated value of K (in Eq. (1)) far exceeds the predicted activity of silicic acid at saturation with each of these phases.

Thus thermodynamic modelling using a reasonable set of potential solid silica phases and widely accepted thermodynamic data [8] indicates that silica 'saturation' with respect to this glass cannot occur as the value of K (4.35×10^{-3}) extrapolated from this data set is nearly double that predicted at saturation with respect to amorphous silica at the test temperature and pH (a value of 2.54×10^{-3}). However, as noted by Fleming [9], the solubility of freshly precipitated silica is approximately double that typically reported in solubility studies with 'aged' amorphous silica.

3.6. The influence of dissolved Al species

As shown in Fig. 2, the lowest dissolution rates in the MW-Si experiments are observed in the experiments conducted with the least concentrated Si-spiked buffer solutions. Where dissolved Al concentrations were quantifiable, rates of dissolution generally decrease as the concentration of dissolved Al increases. These data strongly suggest that the presence of dissolved Al influences the rate of glass dissolution under these experimental conditions. Moreover, it is impossible to rationalize these data with a dissolution rate law based on the activity of orthosilicic acid alone.

One modelling approach is to use a Grambow style rate law that includes an additional term to describe the inhibitory role of Al. Such a rate law may be formulated as follows:

$$r = k_+ \alpha a^{\beta}_{Al_{(inhib)}(aq)}\left(1 - \frac{Q}{K}\right). \tag{2}$$

Here r, k_+, Q and K are the parameters defined in Eq. (1). The additional terms are the activity of the 'inhibitory' Al species ($a_{Al_{(inhib)}}$) and the fitting parameters α and β.

Eq. (2) has been fit to experimental data from the MW-Si and MW-Al experiments using a non-linear regression technique [10]. The resulting 'Al-inhibition model' is

$$r = k_+ \times 1.79 \times 10^{-2}(\pm 3.72 \times 10^{-3}) \times a^{-0.268\pm0.017}_{Al(OH)_4^-(aq)} \times \left(1 - \frac{Q}{K}\right), \tag{3}$$

where the values of k_+ and K are 0.196 (g m^{-2} d^{-1}) and 4.35×10^{-3}, respectively (as in Eq. (1)). The uncertainties in the fitting parameters (α and β) are standard errors in the regressed values. The resulting fit is shown in Fig. 4.

Application of this model produces glass dissolution rates that decrease rapidly as the activity of $Al(OH)_4^-(aq)$ increases at low dissolved Al concentrations. This is in accordance with the results of the MW-Si experiments where rates decrease appreciably in the presence of detectable levels of dissolved aluminium (see Fig. 2). At higher Al concentrations the dissolution rate is less dependent on the $Al(OH)_4^-(aq)$ activity, as observed in the MW-Al experiments. Such an effect can be explained if there are a limited number of reaction sites at the glass surface that may react with the dissolved Al producing aluminosilicate groups that are relatively inert and resistant to dissolution. At higher Al concentrations, all such sites are effectively 'filled' and addition of further Al to the solution does not significantly reduce the glass dissolution rate.

Numerous studies have shown that glass dissolution rates may be influenced by the presence of dissolved Al.

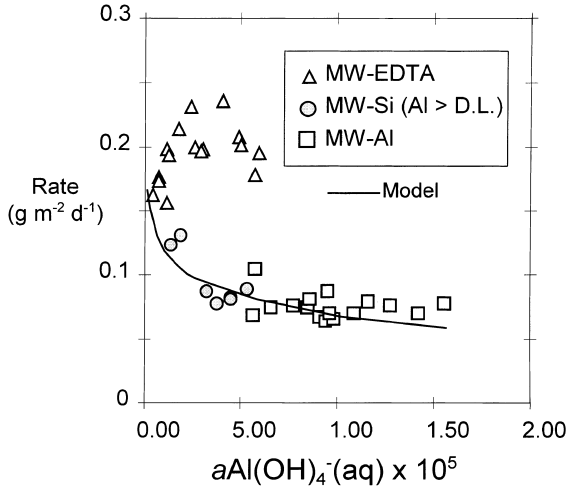

Fig. 4. Rates of glass dissolution (based on steady-state B concentrations) in the MW-Si, MW-Al and MW-EDTA experiments vs the modelled activity of the tetrahydroxyaluminate anion. The line shows predicted rates based on Eq. (3) (see text) fitted to the experimental data obtained in the MW-Si and MW-Al experiments.

In number of models this has been attributed to reaction affinity effects (e.g., [11,12]). However, this cannot be the case when Al is not a glass constituent (e.g., [13]). Also, Al strongly inhibits dissolution of amorphous silica [14]. Thus it seems likely that Al plays an inhibitory role during glass dissolution, although reaction affinity effects cannot be ruled out in the case of glasses containing Al. Spectroscopic studies have shown that dissolved Al reacts with surface silanol sites to form aluminosilicate groups [15]. Formation of such stable groups may effectively passivate reactive sites, leading to reduced glass dissolution rates.

3.7. The influence of EDTA

Experimental studies of glass and mineral dissolution have shown that dissolution may be catalysed by organic ligands that are able to form surface or solution complexes with metallic components. For example, Gin [11] has shown that dissolution of the R7T7 glass is catalysed by organic acids (particularly those containing two or more functional groups).

Data obtained in our MW-EDTA experiments suggest that the presence of 0.005 M EDTA does not directly influence dissolution rates. Observed rates in the MW-EDTA experiments are of a similar magnitude to those in the MW-Si experiments where Al was not detected in the reaction cell output solutions. Thus there is no direct evidence of catalysis by EDTA. However, from examination of Fig. 4 and the tabulated rate data, it would appear that the presence of EDTA reduces the rate influencing effects of dissolved Al. This is likely a reflection of the differing speciation of Al in the MW-EDTA experiments. In the presence of EDTA significant quantities of Al (and other metals) are complexed by this ligand. One possibility is that this 'chelated' Al does not interact with reactive sites at the glass surface and hence does not influence the dissolution rate (i.e., in the presence of EDTA the affinity of Al for the glass surface is effectively reduced).

3.8. Long-term, static, batch dissolution experiments

The results of relatively long-term, static, batch dissolution experiments at 90°C with the MW glass have been reported and analysed by various authors (Zwicky et al. [3], Werme et al. [4], Chambers et al. [5]). Samples of the MW glass were equilibrated with water in polytetrafluoroethane (PTFE) reaction vessels for periods of up to one year. Experiments were conducted with glass monoliths (glass surface area: solution volume ratio $(SA/V) = 10\ m^{-1}$) and glass powders.

During the experiments the concentrations of glass derived solutes increased rapidly until an apparent Si 'saturation' was attained after 91 and 7 days in the monolithic and powder experiments, respectively [3,5]. Following attainment of Si 'saturation', concentrations of soluble glass components (such as B) increased less rapidly.

Forward or initial rates of glass dissolution have been determined from the results of experiments with glass monoliths. Final or 'long-term' dissolution rates have been determined in experiments with glass powders where Si 'saturation' was attained. Values of the initial and final rates were estimated by linear regression of normalised mass losses based on boron vs time in the monolithic and 'Si-saturated' powder experiments. Zwicky et al. [3] report initial glass dissolution rates of 1.1 g m^{-2} d^{-1} and final dissolution rates (under conditions of 'apparent Si saturation') of 0.009 g m^{-2} d^{-1} at 90°C. Thus the final or 'residual' rates calculated from these data are reported to be of the order of 100 times lower than the initial rates [3].

3.9. Comparison of the combined data

Data obtained in the SPFT experiments presented here may be compared directly with those obtained in the MW-F experiments described in Part I, and with the results of the long-term, static, batch dissolution experiments described above.

Fig. 5 is a plot showing dissolution rates in each SPFT experiment vs the activity of silicic acid. This plot illustrates a number of points:

1. Maximal rates are observed in the MW-EDTA experiments where aH_4SiO_4 remains low and in the MW-Si experiments where Al was below ICP-AES detection

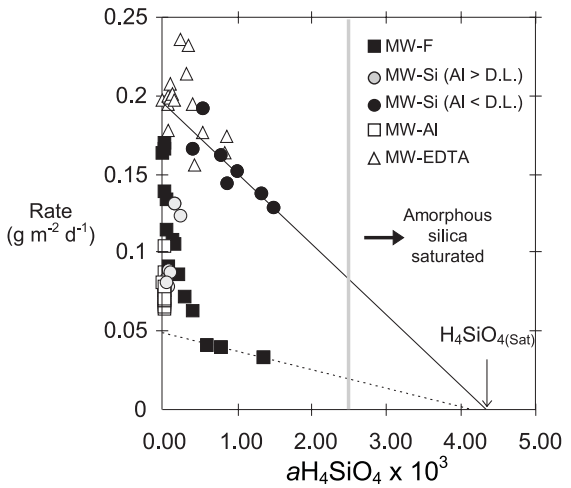

Fig. 5. Comparison of the experimental dissolution rates in the MW-F, MW-Si, MW-Al and MW-EDTA experiments (refer to the key) vs the activity of orthosilicic acid. The solid line shows a linear regression through the MW-Si data obtained in tests where Al was below the ICP-AES detection limits (Al < DL). The dashed line shows a linear regression through the MW-F data for tests in which Al was below the ICP-AES detection limits. The vertical line indicates amorphous silica saturation at pH 9.38 (40°C) (see text).

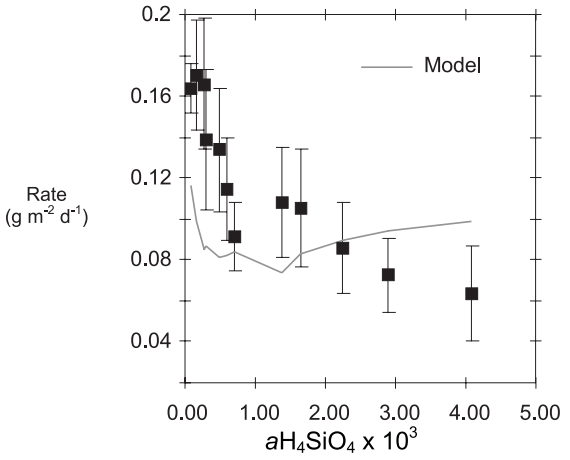

Fig. 6. Rates of glass dissolution (based on steady-state B concentrations) in the MW-F experiments vs the activity of orthosilicic acid. Model line shows predicted rates based on the Al inhibition model (Eq. (3)).

limits. Extrapolating the linear trends shown in Fig. 3 predicts zero dissolution rates at silicic acid activities far in excess of those predicted at saturation with amorphous silica.

2. Comparable rates are observed in the MW-F, MW-Si and MW-Al experiments where Al was detected in the leachate. It would appear that the presence of dissolved Al (in the absence of EDTA) strongly reduces the dissolution rate under these experimental conditions.
3. The lowest rates are observed in the MW-F_13–MW-F_15 experiments. Here, Al was below detection limits and reaction cell solutions were relatively concentrated with glass derived solutes. Gel development was comparatively extensive in these tests.

The results of the MW-Al experiments indicate that the presence of small quantities of Al significantly suppresses the glass dissolution rate in systems where the silicic acid activity is also very low. On the contrary, the presence of relatively large amounts of dissolved silica in the absence of significant quantities of dissolved Al leads to only a small suppression of the dissolution rates in the MW-Si experiments. Thus under these experimental conditions, it would appear that Al has a far more significant effect on the glass dissolution rate than silicic acid on a 'mole per mole' basis.

The Al-inhibition model has also been applied to the data obtained in the MW-F experiments, as shown in Fig. 6. The model (Eq. (3)), parameterised by fitting data obtained in the MW-Si and MW-Al experiments, does not provide good agreement with the MW-F data set.

As discussed in Part I, data from the MW-F experiments are consistent with a glass dissolution rate law that includes a mixed Al/Si 'affinity' term. Fig. 7 shows rate data from the MW-Al and MW-Si experiments plotted along with the MW-F data vs a Al · Si product term. In these plots, the trendlines are linear regressions through the MW-F data, and are the predicted dissolution rates based on the rate laws discussed in Part I.

In Fig. 7(a) the pH-corrected rate values are plotted vs the activity product $a^{0.06}_{Al(OH)^-_4(aq)} \cdot a^{0.51}_{H_4SiO_4}$. The trendline gives predicted dissolution rates based on the following rate law, which has been parameterised using data obtained in the MW-F experiments, as described in Part I

$$R = R_0\left(1 - \frac{a^{0.06}_{Al(OH)^-_4(aq)} a^{0.51}_{H_4SiO_4}}{K_{Al\cdot Si}}\right), \quad (4)$$

where R is the rate of glass dissolution (g m^{-2} d^{-1}), R_0 the apparent rate constant under these experimental conditions (40°C, pH 9.38) and $K_{Al\cdot Si}$ is a constant defined as the activity product $a^{0.06}_{Al(OH)^-_4(aq)} \cdot a^{0.51}_{H_4SiO_4}$ which corresponds to a hypothetical zero rate of dissolution (not observed experimentally). Values of R_0 and $K_{Al\cdot Si}$ estimated from these data by linear regression are $R_0 = 0.183 \pm 0.006$ g m^{-2} d^{-1} and $K_{Al\cdot Si} = 0.012 \pm 0.001$. This provides reasonable agreement in the case of the MW-Si data, but somewhat over-predicts the dissolution rates in the MW-Al experiments.

The calculated activities and pH-corrected rate values are subject to the combined uncertainties in the geochemical modelling calculations and the dissolution rate pH correction procedure. Fig. 7(b) compares

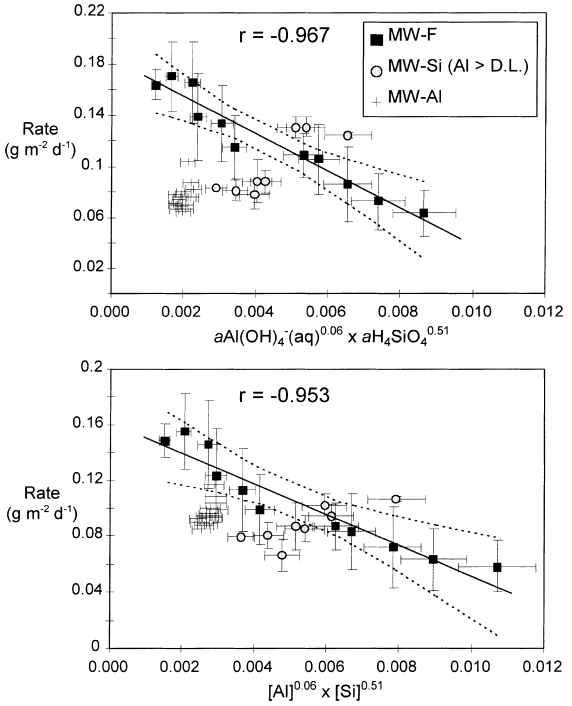

Fig. 7. Rates of glass dissolution (based on steady-state B concentrations) in the MW-F, MW-Al and MW-Si experiments. The plots show: (a) pH-corrected rates vs the activity product term and (b) non-pH-corrected rates vs the concentration product terms (see text and Part I). Linear regression trendlines are drawn through the MW-F data only. The dashed lines are 95% confidence limits about the regression line and r values are the product moment correlation coefficients.

non-pH-corrected rates with the molar concentration product $[Al]^{0.06}[Si]^{0.51}$. The corresponding rate law takes the form

$$R = R_0\left(1 - \frac{[Al]^{0.06}[Si]^{0.51}}{K_{Al\cdot Si}}\right), \quad (5)$$

where values of R_0 and $K_{Al\cdot Si}$ are estimated by linear regression at 0.162 ± 0.007 g m^{-2} d^{-1} and 0.014 ± 0.001, respectively. There is reasonable agreement between the combined experimental data and predicted rates when non-pH-corrected rates and the molar concentration product $[Al]^{0.06}[Si]^{0.51}$ are considered. The mixed Al/Si rate laws are certainly more consistent with the combined rate data than Eq. (1).

It is useful to compare the results of the MW-F_15 and the MW-Si_16 experiments. In the MW-F_15 and MW-Si_16 experiments the Si concentration in the output solution was 55 mg l^{-1}. The B release rate in the MW-F_15 experiment was 4 times lower than that in the MW-Si_16 experiment even though Si concentrations are comparable and Al concentrations are low (below detection limits) in each case. The principal difference between these two tests was that the MW-Si_16 experiment was run at q/s ratio approximately 125 times larger than the MW-F_15 test. Consequently, the concentration of other glass-derived solutes was much lower in the MW-Si_16 test as compared with the MW-F_15 test.

The experiments described here were designed to investigate specifically the rate influencing effects of dissolved Al and Si. It should be noted that this complex glass also contains a variety of minor components, including REE (Nd, Ce, La), Sr and Zr. Note that in the MW-F experiments (described in Part I), the reaction cell solutions become 'concentrated' with glass derived solutes, particularly at low q/s ratios. One possibility is that these minor elements also influence the glass dissolution process by contributing to the reaction 'affinity' or by surface reactions at reactive sites. Further, systematic experiments would be required to fully evaluate this possibility.

Long-term experiments with this and other glass formulations in static batch reactors indicate that long term rates of dissolution in quasi-saturated systems are considerably lower than forward dissolution rates, typically by factors of between 100 and 1000 times [16]. 'Forward' and 'final' rates of dissolution in long-term, static, batch dissolution experiments with this glass formulation are reported to differ by a factor of 100 at 90°C [3].

Note that in the SPFT experiments the lowest dissolution rates were observed in the MW-F experiments conducted at the lowest q/s ratios (MW-F_13–MW-F_15). The highest dissolution rate was 0.235 ± 0.046 (MW-EDTA_11) and the lowest was 0.033 ± 0.006 g m^{-2} d^{-1} (MW-F_15). Thus dissolution rates in the flow-through experiments described in this work vary by a maximum factor of 7. In the context of a rate law containing an affinity term, and assuming a forward dissolution rate of 0.183 ± 0.006 g m^{-2} d^{-1}, this lower rate corresponds with 86% saturation with respect to the rate limiting reaction. The residual rate reported for this glass in the 90°C static, batch dissolution experiments described above (0.009 g m^{-2} d^{-1}) represents 99% saturation compared to the reported forward dissolution rate (1.1 g m^{-2} d^{-1}) [3]. This level of saturation is not approached in the SPFT experiments described here as a result of the solution flow-through.

4. Conclusions

The results presented here indicate that both dissolved Si and Al influence the dissolution rate of this complex borosilicate glass. It has been demonstrated that the rate influencing effects of dissolved Al are far

more significant than those of Si on a mole per mole basis under these experimental conditions (40°C, moderately alkaline media). Complexation of Al by EDTA reduces the rate influencing effects of dissolved aluminium. In these experimental systems, Al solubility is limited as a result of the formation of secondary gels. These findings indicate that processes which moderate Al solubility or aqueous speciation (such as secondary phase development or the presence of organic ligands) are likely to influence the dissolution rate of this glass.

The experimental results presented here further substantiate the conclusions drawn in Part I. A rate law containing only the activity of silicic acid, such as the model proposed by Grambow [7], is likely to over predict dissolution rates in systems where dissolved Al is present in significant concentrations and where Al speciation is not influenced by chelating ligands such as EDTA. The combined data is generally consistent with glass dissolution rate laws of the form given by Eqs. (4) and (5). It is impossible to rationalize the experimental data with a dissolution rate law based on the activity of orthosilicic acid alone.

These conclusions are based on data obtained in relatively short-term, dynamic experiments (maximum duration 19 days). The rates are likely to exceed those obtained in long-term, static tests where significantly reduced rates are typically observed. The validity of the rate laws has only been demonstrated in short-term experiments in mildly alkaline media at 40°C. Care must be taken when extrapolating this behaviour to a potential repository environment. In such a system, it is envisaged that the glass will eventually contact relatively slow moving groundwaters. Unless secondary phases form that accelerate the glass reaction rate by lowering the solution activities of dissolved Si and Al species, long-term dissolution rates under such quasi-static conditions may be notably lower than those reported here (as in long-term, static, batch dissolution experiments where near 'saturation' conditions are attained). Such rate laws would be conservative when applied in a repository performance assessment context since overestimated waste glass dissolution rates would likely result in an overestimate of the associated risk.

Acknowledgements

This work was conducted at the Battelle Pacific Northwest National Laboratory (PNNL) and was financially supported by British Nuclear Fuels plc. and Associated Western Universities, Inc. under a grant with the US Department of Energy. The assistance of numerous people (particularly Toni Owen, Karl Pool, May-Lin Thomas and Jim Young) with various aspects of the experimental work is greatly appreciated.

References

[1] B.P. McGrail, W.L. Ebert, A.J. Bakel, D.K. Peeler, J. Nucl. Mater. 249 (1997) 175.
[2] P.K. Abraitis, B.P. McGrail, D.P. Trivedi, F.R. Livens, D.J. Vaughan, this issue, p. 196.
[3] U. Zwicky, B. Grambow, C. Magrabi, E.T. Aerne, R. Bradley, B. Barnes, Th. Graber, M. Mohos, L.O. Werme, Mater. Res. Soc. Symp. Proc. 127 (1989) 129.
[4] L. Werme, I.K. Bjorner, G. Bart, U. Zwicky, B. Grambow, W. Lutze, R.C. Ewing, C. Magrabi, J. Mater. Res. 5 (1990) 1130.
[5] A.V. Chambers, T.G. Heath, C.M. Linklater, A.M. Thompson, R.M. Wiggin, Mater. Res. Soc. Symp. Proc. 506 (1998) 391.
[6] D.L. Parkhurst, US Geological Survey, Water-Resources Investigations Report 95-4227, 1995.
[7] B. Grambow, Mater. Res. Symp. Proc. 44 (1985) 209.
[8] D.K. Nordstrom, L.N. Plummer, D. Langmuir, E. Busenberg, H.M. May, B.F. Jones, D.L. Parkhurst, in: Chemical Modeling of Aqueous Systems II, American Chemical Society Symposium Series 416, Washington, 1996, p. 398, (chapter 31).
[9] B.A. Fleming, J. Colloid Interface Sci. 110 (1986) 40.
[10] D.W. Marquardt, J. Soc. Indust. Appl. Math. 11 (1963) 431.
[11] S. Gin, Mater. Res. Symp. Proc. 412 (1996) 189.
[12] V. Daux, C. Guy, T. Advocat, J.L. Crovisier, P. Stille, Chem. Geol. 142 (1997) 109.
[13] M.F. Dilmore, D.E. Clark, L.L. Hench, Am. Ceram. Soc. Bull. 58 (11) (1979) 1111.
[14] R. Iler, J. Colloid Interface Sci. 43 (1973) 399.
[15] W.E.E. Stone, G.M.S. El-Shafei, J. Sanz, S.A. Selim, J. Phys. Chem. 97 (1993) 10127.
[16] W.L. Ebert, J.J. Mazer, Mater. Res. Soc. Symp. Proc. 333 (1994) 27.
[17] K. Pool, personal communication (1998).